Scanning tunneling microscopy. II. Calculation of images of atomic and molecular adsorbates

F. Biscarini* and C. Bustamante
Department of Chemistry and Institute of Molecular Biology, University of Oregon, Eugene, Oregon 97403

V. M. Kenkre
Department of Physics and Astronomy, University of New Mexico, Albuquerque, New Mexico 87131
(Received 22 July 1994)

A theory of the scanning-tunneling-microscopy (STM) current of adsorbates with focus on effects of coherence in electron motion in the STM junction has been developed in the preceding paper [Phys. Rev. B **51**, 11 074 (1995)]. That theory is illustrated through an application to the computation of several realistic STM images. The tip, the substrate, and the adsorbate are treated as finite clusters of atoms. Extended Hückel theory is used to calculate the STM current. The substrate used is Au (111). Images that can be compared directly with experimental observations are constructed for the bare Au (111) surface as well as for atomic and molecular adsorbates. The atomic adsorbates treated are Au, Na, H, C, and O. The molecular adsorbates treated are O_2, CO, and benzene. A comparison is made with observations reported in the literature and agreement with a number of features is found. Our calculated images suggest that observations of giant corrugation in STM of metals might be arising from nonperturbative electron transport between localized surface states. Nontopographical artifacts due to adsorbates and the dependence of the image on the tip-sample separation are discussed.

I. INTRODUCTION

A theoretical formalism for the interpretation of scanning-tunneling-microscopy (STM) images has been presented in the preceding paper,[1] referred to hereafter as I, with special attention given to the effects of adsorbate molecules placed in the tip-substrate gap. Basic issues and simple illustrations of the theory have been given in I. The present paper constitutes a detailed application of the theory to realistic situations. Images are constructed on the basis of the theory in I in a form that makes a direct comparison to experimental observations possible. Such a comparison is then made and shown to result in a number of insights into the mechanism of contrast of adsorbed molecules.

The paper is organized as follows. In the rest of this section, the calculational details that go into the present application of the theory of I are presented. Sections II–IV contain applications of the theory to various situations and Sec. V constitutes a discussion. The substrate in all cases considered is Au(111). In Sec. II, images of bare Au(111) surfaces are calculated, convergence issues of the calculational methods are discussed, and a comparison to the experiments of Hallmark *et al.*[2] is made. Atomic adsorbates are treated in Sec. III and molecular adsorbates in Sec. IV. Images of atomic adsorbates calculated in Sec. III include those for Au, Na, and H on the one hand and for C and O on the other. The former allow us to analyze energy mismatch features and make contact with the simulations of Lang,[3] while the latter, involving more complex adatoms, permit us to address the experimental findings of Brune *et al.*[4,5] and Kopatzki and Behm[6] and the theoretical interpretation given by Doyen *et al.*[7] Molecular adsorbates studied in Sec. IV include O_2, which is relevant to investigations of early stages of surface oxidation by Ruan *et al.*,[8] CO, which has been studied experimentally by Zeppenfeld, Lutz, and Eigler,[9] and the more complex benzene molecule investigated by Ohtani *et al.*[10]

We study the STM junction by modeling it as a finite cluster of atoms. For a given tip-substrate-molecule configuration, each atom has a fixed position and is represented by localized atomic orbitals. Each orbital representing an atom of the tip or substrate exchanges particles with the reservoir and our generalized expression for the STM current, derived as Eq. (2.2) in I, applies:

$$I=\frac{en_e}{2}\left\{\frac{\Delta\eta_T^{\rm th}}{\int_0^{+\infty}dt\,[\Pi_{TT}(t)-\Pi_{TS}(t)]}-\frac{\Delta\eta_S^{\rm th}}{\int_0^{+\infty}dt\,[\Pi_{SS}(t)-\Pi_{ST}(t)]}\right\}. \tag{1.1}$$

Here e is the electron charge magnitude, n_e is the number of electrons in the STM junction determined by the equilibrium chemical potential μ of the system, Π's averages of probability propagators that describe electron motion in the absence of driving reservoirs, and $\Delta\eta_T^{\rm th}=\eta_T^{\rm th}-P_T^{\rm th}$, where $\eta_T^{\rm th}$ is the electron probability at the tip in the absence of a driving agency and $P_T^{\rm th}$ is the quasiequilibrium population imposed by the reservoir in contact with the tip. The labels T and S denote averages over the group of atomic orbitals $|\tau\rangle$ and $|\sigma\rangle$ representing the tip and the substrate, respectively. Further details may be found in I.

The images we calculate are obtained through an evaluation of (1.1). We fix the number of electrons in the cluster and take the chemical potential μ close to the energy of the highest occupied molecular orbital (HOMO). With the help of the fact that the two contributions inside the large curly brackets in (1.1) are equal to each other (see I), we determine the chemical potentials μ_T and $\mu_S=\mu_T+e\phi_{TS}$ of the driving reservoirs. For a system with a discrete number of states, the equality of the two terms in (1.1) can be expressed as

$$\frac{\sum_{\tau}\sum_{m}|\langle\tau|m\rangle|^2\left[\mathrm{erf}\left[\frac{E_m-\mu}{\sqrt{2}\delta}\right]-\mathrm{erf}\left[\frac{E_m-\mu_T}{\sqrt{2}\delta}\right]\right]}{\int_0^\infty dt\,[\Pi_{TT}-\Pi_{TS}](t)} = -\frac{\sum_{\sigma}\sum_{m}|\langle\sigma|m\rangle|^2\left[\mathrm{erf}\left[\frac{E_m-\mu}{\sqrt{2}\delta}\right]-\mathrm{erf}\left[\frac{E_m-\mu_T-e\phi_{TS}}{\sqrt{2}\delta}\right]\right]}{\int_0^\infty dt\,[\Pi_{SS}-\Pi_{ST}](t)} . \quad (1.2)$$

Here the sums over m are on the cluster eigenstates with energy E_m and the norm square quantities, which we approximate as Mulliken populations,[11] are projections of the eigenstates $|m\rangle$ of the cluster onto the atomic orbitals. The error function differences arise from Gaussian broadening of the density of states (we use a standard deviation $\delta=0.5/\sqrt{2}$ eV) integrated on finite energy windows $[\mu,\mu_T]$ and $[\mu_S,\mu]$ for a positive tip bias voltage. The chemical potential μ_T that satisfies (1.2) is determined numerically and the current is calculated from (1.1). The average propagator integrals are calculated from their microscopic counterparts as

$$\int_0^\infty dt\,[\Pi_{TT}-\Pi_{TS}](t)\approx\frac{\sum_{\tau}\sum_{\tau'}\tilde{\Pi}_{\tau\tau'}(0)w_{\tau'}}{\sum_{\tau}w_{\tau}} - \frac{\sum_{\tau}\sum_{\sigma}\tilde{\Pi}_{\tau\sigma}(0)w_{\sigma}}{\sum_{\sigma}w_{\sigma}} , \quad (1.3)$$

as given in Eq. (3.18) of I. Here tildes indicate Laplace transforms and the weights w are taken as

$$w_{\tau}=\sum_{m}\left[\mathrm{erf}\left[\frac{E_m-\mu_T-e\phi_{TS}}{\sqrt{2}\sigma}\right]-\mathrm{erf}\left[\frac{E_m-\mu_T}{\sqrt{2}\sigma}\right]\right]|\langle\tau|m\rangle|^2 , \quad (1.4)$$

i.e., as projected fractions of states within the energy window $\mu_S-\mu_T$. The other relevant propagator integral is obtained by permuting the T and S labels in (1.3) and (1.4).

The calculation of the electronic structure of the cluster is carried out with the help of extended Hückel theory (EHT).[12] The choice is motivated by the simplicity of the method, by the fact that it allows us to treat the tip-substrate-adsorbate configuration as a single entity and by its ability to provide physical insights in STM problems.[13] If required, it is straightforward to replace the EHT, at least in principle, by more rigorous electronic-structure theories such as density-functional theory.[14] Although EHT is based on a nonorthogonal basis set of Slater-type orbitals (STO's), we have adapted it to the calculation of probability propagators between orthogonal localized states, as discussed in Sec. III.

For the purpose of introducing bath effects on the STM current in cluster models, we have chosen the simple tool of the stochastic Liouville equation (SLE) in light of the extensive analysis and insight available in the literature on exciton dynamics in molecular aggregates.[15] The SLE is

$$\frac{d(\rho_{mn}(t)-\rho^{\mathrm{th}}_{mn})}{dt}=-i[H,\rho(t)-\rho^{\mathrm{th}}]_{mn} +(1-\delta_{mn})\alpha(\rho_{mn}(t)-\rho^{\mathrm{th}}_{mn}) , \quad (1.5)$$

where $\rho(t)-\rho^{\mathrm{th}}$ is the deviation of the density matrix of the electron from the equilibrium (thermal) density matrix, H is the Hamiltonian of the system, square brackets indicate the commutator, α is the dephasing rate, δ is Kronecker's delta, and we have set $h/2\pi=1$, with h being Planck's constant. The first term on the right-hand side describes the coherent motion of the electron and the second term introduces the effect of bath interactions in the form of destruction of off-diagonal elements of the density matrix at a constant rate α. The basis set in (1.5) is made of localized orthogonal states. We refer the interested reader to Ref. 15 for the origin and physical meaning of the SLE. Suffice it to state here that the dephasing rate α (the rate at which spatial coherence in transport is destroyed as a result of reservoir interactions) provides a simple but convenient way of describing with continuity coherent and incoherent motion. It is simply related (inversely proportional) to the density of states factor in the Fermi golden rule. The SLE has appeared in numerous places, e.g., in the form of the relaxation time approximation as discussed by Wannier.[16]

We calculate the propagators Π by means of a simple

algorithm that exploits the well-known relation in the Laplace domain between propagators and memory functions W:

$$\tilde{\mathbf{\Pi}}(\varepsilon)=\frac{1}{\varepsilon\mathbf{I}-\tilde{\mathbf{W}}(\varepsilon)} , \tag{1.6}$$

where ε is the Laplace variable, $\mathbf{I}$ is the identity matrix, and the diagonal element of the memory functions stands for $\tilde{W}_{mm}(\varepsilon)=-\sum_{n\neq m}\tilde{W}_{nm}(\varepsilon)$. The Laplace transformed memory functions can be shown[17] to follow directly from the coherent propagator:

$$\tilde{\mathbf{W}}(\varepsilon)=(\varepsilon+\alpha)\mathbf{I}-\frac{1}{\tilde{\mathbf{\Pi}}^{\rm coh}(\varepsilon+\alpha)} . \tag{1.7}$$

The propagator integrals (1.3) cannot be obtained by inversion of $\tilde{\mathbf{W}}(0)$ because the matrix of the memory functions is singular in the limit $\varepsilon\rightarrow 0$. This singularity is removed by introducing the conservation of the populations in the cluster. From a practical standpoint, a memory function difference matrix $\Delta\tilde{\mathbf{W}}(0)$ is constructed by the elimination of a row and subtraction of a column, say the Nth (N being the dimension of the basis set), from the other $N-1$ columns. The matrix elements of $\Delta\tilde{\mathbf{W}}(0)$ are $\Delta\tilde{W}_{mn}(0)=\tilde{W}_{mn}(0)-\tilde{W}_{mN}(0)$. It is straightforward to show that the relevant differences of the propagator integrals in Eq. (1.1) follow directly from

$$\int_0^\infty dt[\Pi_{\tau\tau'}-\Pi_{\tau\sigma}](t)=\left[\frac{1}{\Delta\tilde{\mathbf{W}}(0)}\right]_{\tau\sigma}-\left[\frac{1}{\Delta\tilde{\mathbf{W}}(0)}\right]_{\tau\tau'} , \tag{1.8a}$$

$$\int_0^\infty dt[\Pi_{\sigma\sigma'}-\Pi_{\sigma\tau}](t)=\left[\frac{1}{\Delta\tilde{\mathbf{W}}(0)}\right]_{\sigma\tau}-\left[\frac{1}{\Delta\tilde{\mathbf{W}}(0)}\right]_{\sigma\sigma'} \tag{1.8b}$$

and from the averaging procedure (1.3).

The coherent propagators $\tilde{\mathbf{\Pi}}^{\rm coh}(\varepsilon+\alpha)$, defined as the Laplace transformed Green's function of (1.5) in the absence of bath effects, can be calculated in terms of the energies and eigenstates of the cluster as

$$\tilde{\Pi}^{\rm coh}_{\tau\sigma}(\varepsilon+\alpha)=\sum_m\frac{|\langle\tau|m\rangle|^2|\langle m|\sigma\rangle|^2}{\varepsilon+\alpha}+2\sum_m\sum_{n>m}\langle\tau|m\rangle\langle m|\sigma\rangle\langle\sigma|n\rangle\langle n|\tau\rangle\times\frac{(\varepsilon+\alpha)}{(\varepsilon+\alpha)^2+(E_m-E_n)^2} . \tag{1.9}$$

The summation is over the cluster (the tip-substrate-adsorbate combination) eigenstates. The quantity $\langle\tau|m\rangle$ coincides with the coefficient $C_{\tau m}$ of the basis set orbital τ in the expansion of the eigenstate m, when the basis set orbitals are orthonormal. This is not the case for EHT. We therefore calculate the propagator (1.9) via an approximation procedure that accounts for the overlap between atomic orbitals and, at the same time, preserves symmetry and normalization properties of the coherent propagator. The fact that the overlap $\mathbf{S}$ is diagonalized by the solution $\mathbf{C}$ of the generalized secular problem

$$\sum_\nu\sum_\mu C_{\nu n}S_{\nu\mu}C_{\mu m}=\delta_{mn} , \tag{1.10}$$

suggests that we define

$$\langle\mu|m\rangle\langle m|\mu\rangle\approx\sum_\nu C_{\mu m}S_{\mu\nu}C_{\nu m} , \tag{1.11a}$$

$$\langle\mu|n\rangle\langle m|\mu\rangle\approx\sum_\nu C_{\mu m}S_{\mu\nu}C_{\nu n} . \tag{1.11b}$$

Equation (1.11a) involves the projection coefficients proposed by Mulliken[11] for the evaluation of gross populations and consists of a linear approximation in the overlap to the Wannier state populations. These definitions clearly satisfy the constraints on the propagator (1.9). Furthermore, it can be easily shown that, in the case of a nonorthogonal dimer, the relevant propagator integral is proportional to $V_{\rm eff}^2$, where $V_{\rm eff}$ is given by $H/(1-S^2)$, H being the Hamiltonian matrix element and S the overlap between the orbitals. Such a relation would also hold for a dimer of orthogonal localized states coupled by the matrix element $V_{\rm eff}$.[18]

The algorithm currently implemented in our program for the simulation of images and other STM observables consists of the following steps: (i) generating the positions of the atoms in the cluster, (ii) solving the generalized secular equation $(\mathbf{H}-\mathbf{ES})\mathbf{C}=\mathbf{0}$, where $\mathbf{H}$ is given by EHT, (iii) calculating the coherent propagator (1.9) for a given α with the approximations (1.11), (iv) calculating the relevant propagator integrals with (1.7) and (1.8), (v) solving for μ_T in (1.2), and (vi) calculating the current (1.1). We use a basis set of 200 single-ζ STO orbitals. The current at each scanned point is acquired in about 2 min CPU on an IBM RISC 6000/530H with optimized code. The images presented in this paper have been produced with the help of 20×20 and 30×30 point grids with no symmetry simplifications. With the present configuration, we can handle a basis set of up to 650 orbitals. The maximum number of atoms we can analyze in transition-metal clusters is therefore less than 100 if we adopt the full valence-shell atomic basis set (nine functions) or a few hundred if only s orbitals are considered in the representation. Although the latter choice does not describe properly those systems in which d orbitals and open-shell configurations are important (e.g., chemisorption systems), these simplified cluster models serve to produce STM observables that can be related to experimental results in a straightforward manner. In the following sections, we model the atomically flat Au(111) with clusters of different size, in which each atom is represented in terms of a single s orbital per atom. Our calculations do not show substantial variations when Au $5d$ and $6p$ orbitals are added to the basis set.

II. IMAGES OF THE BARE Au(111) SURFACE

The first object we study through our theoretical image calculations is the bare Au(111) cluster. Our choice is dictated by the fact that we can compare our predictions with some fundamental experimental results,[2] which have shown the capability of STM to provide atomic resolution on low-index metal surfaces. The experimental

TABLE I. EHT screening parameters (ξ_1,ξ_2), double-ζ coefficients (c_1,c_2), and ionization potentials (IP) for W and Au Slater-type orbitals.

	W					Au				
Orbital	ξ_1	ξ_2	c_1	c_2	IP	ξ_1	ξ_2	c_1	c_2	IP
6*s*	2.341		1.0		−8.26	2.602		1.0		−9.22
6*p*	2.309		1.0		−5.17	2.584		1.0		−5.55
5*d*	4.982	2.068	0.694	0.5631	−10.37	6.163	2.794	0.6851	0.5696	−15.76

results have also prompted theoretical studies[19] on the origin of the giant corrugation observed. In all our calculations, the laboratory z axis is taken along the direction normal to the surface, so that the distance between the tip apex atom and the plane of Au atoms represents the tip z coordinate measured from the uppermost plane of substrate atoms. The x axis is taken along the [110] direction, i.e., it coincides with one of the surface lattice vectors. The central atom of the atomically flat surface sets the origin of the laboratory frame.

Extended Hückel parameters fitted to bulk and molecular properties[20] or from Hartree-Fock double-ζ wave functions[21] have been adopted for single-ζ and double-ζ Slater-type orbitals. Table I shows the values of these parameters in the case of tungsten and gold. The rate α has been chosen to be on the order of normal tight-binding matrix elements, viz., 1 eV, and it results in intermediate coherence. We have assessed the range of appropriate values of this rate by evaluating the stability in the corrugation of the Au(111) surface for a given cluster size. Thus, for the clusters used in the calculations related to Table II, values in the range 0.1–1 eV satisfied the stability requirement, while the value 0.01 led to largely inequivalent extrema being produced in most of the tip models. While somewhat arbitrary, the value chosen has been selected particularly for its compatibility with the observations and its ability to illustrate consequences of intermediate coherence. Unless otherwise specified, the bias voltage is 20 mV and the temperature is 4 K. Consequently, nontopographical features are primarily ascribed to quantum interference effects. We calculate the chemical potential μ under the assumption that the junction is not charged, which implies that the number of electrons populating the eigenstates equals the overall number of valence electrons of the atoms in the cluster.

For simplicity, we have taken the tip to consist of a single Au atom. Our studies of larger tips have not shown much qualitative difference in the calculated images. Incidentally, we have carried out a systematic investigation of the effect of tip size in the context of observations of giant corrugations.

In order to avoid artifacts arising from the finite size of the cluster, we first study, in Sec. II A below, the extent to which our calculations are affected by lateral extension of the substrate and the number of inner layers. We also monitor the convergence of the density of states with cluster size. This preliminary study is then used in Sec. II B to select optimal cluster sizes for the actual calculations of images.

A. Convergence of results with lateral substrate size and influence of inner layers

We study the dependence of a single two-dimensional layer of Au(111) containing all the neighbor atoms within a radius $r=6$, 9, 12, 14.5, and 17.4 Å from the central atom, i.e., 19, 37, 61, 91, and 127 atoms, respectively. The tip scans at $z=4$ Å along the x axis in the range [0,4] Å, so that the signal is acquired above the central atom at (0,0,0) Å and the nearest neighbor at (2.884,0,0) Å. In a periodic system, these two atoms would be equivalent. The current profiles in Fig. 1(a) show the convergence of both the positions of the extrema and the corrugation as the size increases. Boundary effects become barely noticeable for clusters larger than Au_{37}. Modulation of the current [the right-hand axis in Fig. 1(b)] is approximately ±25–30 % of the average signal $\langle I \rangle$, estimated as the mean between the absolute maximum and minimum current. This should be compared with the observed value[2] of ±10%. In terms of a Fourier analysis of the signal restricted to the lowest reciprocal-space vectors, $\langle I \rangle$ would be the zero-frequency Fourier component. The value of $\langle I \rangle$ exhibits a tendency to decrease as the cluster lateral size increases, but its variation is less than one order of magnitude [the left-hand axis in Fig. 1(b)]. In terms of topographical corrugation, the fluctuations among the values reported on the right-hand axis of Fig. 1(b) correspond to variations below the accuracy of a UHV STM, viz., 0.05 Å. This is estimated from the rule of thumb $\Delta z = z_+ - z_- \approx \ln(I_{\max}/I_{\min})/2\kappa$, where z_+ and z_- are maximum and minimum tip-substrate separations at constant current and 2κ is the exponential decay rate of the average signal $\langle I \rangle$. For Au_{127}, the best fit value of κ is 2.77 $Å^{-1}$. This value is approximately twice the Au 6*s* orbital screening coefficient ($\zeta=2.602$ a.u.) and leads to differences in topographical corrugation of at most 0.02 Å for the clusters in Fig. 1.

While for small clusters [Fig. 1(c)] we notice a size dependence in the density of states, the dependence ceases to be noticeable for clusters larger than Au_{127}. The surface bandwidth is approximately 8 eV. The Fermi level [vertical line in Fig. 1(c)] that we take as the energy of the HOMO of the neutral substrate undergoes a slight shift towards higher values with a size increase and reaches approximately −8.4 eV with respect to the vacuum level in the case of Au_{127}. While this is about twice the experimental value of the work function (−4.3 eV), the tendency is consistent with the EHT parametrization chosen for the Hamiltonian diagonal matrix elements and

is compatible with standard values[20] of screening coefficients for metal atom orbitals.

In order to rule out possible effects from missing inner layers in the single-layer model of the substrate, we have calculated the constant-height current at $z=4$ Å for clusters built by augmenting the Au_{61} cluster with inner layers in an *ABCA* stacking sequence (clusters Au_{61}, Au_{122}, Au_{183}, and Au_{244}, respectively) [Fig. 2(a)]. The corrugation is comparable to that shown in Fig. 1(b) for the single-layer cluster and appears rather stable with the number of layers [Fig. 2(b)]. This result agrees with the idea[22] that STM is a probe of the top layers. Notice also that the density of states converges properly towards the parabolic shape, which is characteristic of a band originated by *s* orbitals in a three-dimensional lattice [Fig. 2(c)].[23] The energy spread of the density of states is approximately 14 eV.

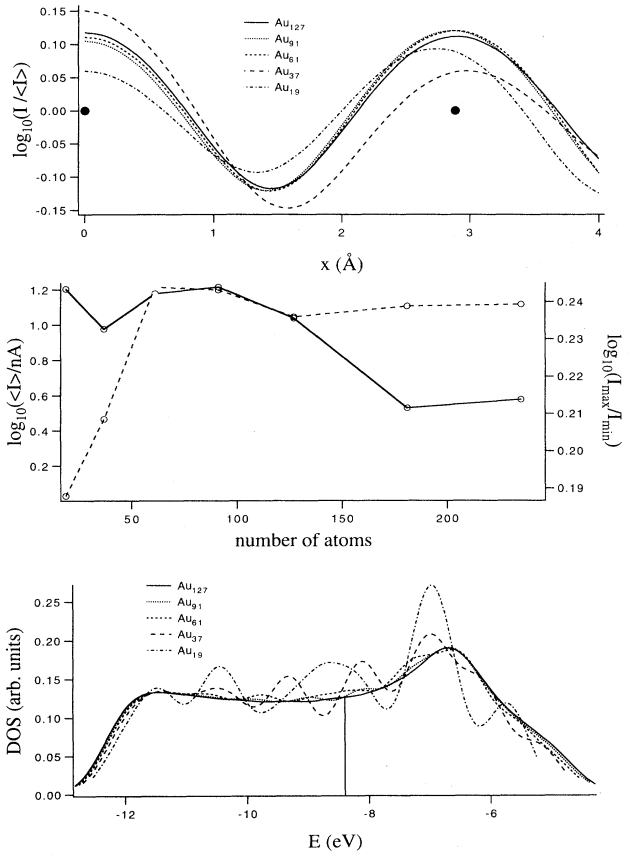

FIG. 1. Effects of enlarging the cluster lateral size on (a) the position of the extrema, (b) the base-line current (left axis) and the corrugation (right axis), and (c) the substrate density of states. The substrate is modeled as a single-layer Au_n cluster, with $N=19,37,61,91,127$. Here, as in Figs. 2–5 and 8–12, the value of α has been taken to be equal to 1 eV and the temperature to be 4 K. The base-line current $\langle I \rangle$ and the corrugation are, respectively, half the sum of and the ratio between the maxima and the minima of current. The single-atom Au tip scans 4 Å above the plane of Au atoms, along the [110] direction. The lattice spacing is 2.88 Å. The vertical bar in (c) marks the substrate Fermi level of Au_{127}.

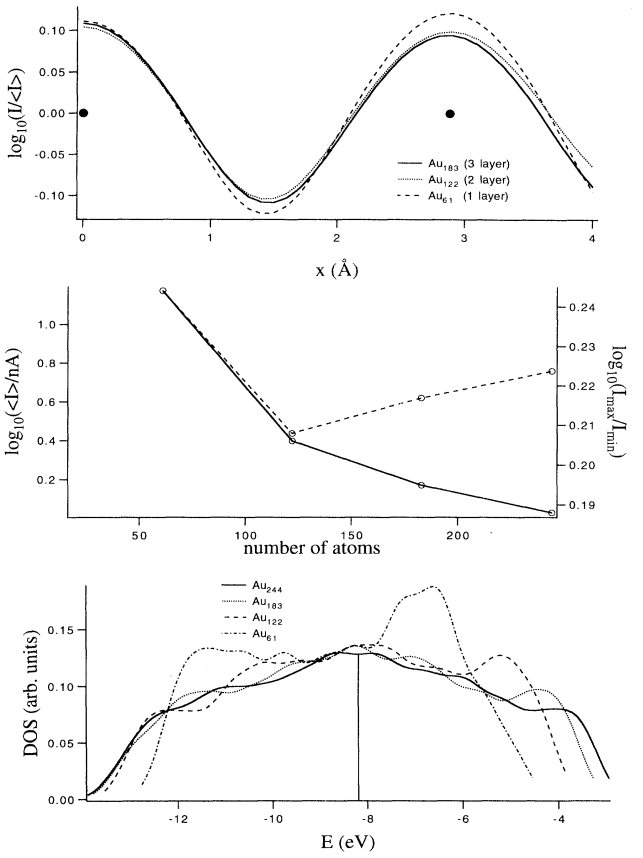

FIG. 2. Influence of inner layers on (a) the position of the extrema, (b) the base-line current (left axis) and the corrugation (right axis), and (c) the substrate density of states. The substrate is taken as an *n*-layer Au cluster, with $n=1,2,3,4$ with 61 atoms for each layer.

The conclusion to be drawn from the above results is that it is reasonable to employ clusters of size Au_{61} and at most one inner layer for our STM investigations.

B. Calculation of images: Atomic resolution in Au(111) and coherence effects

Having assessed the dependence of our results on the size of the bare substrate, we now proceed to calculate images and topographical corrugations for clusters larger or equal to Au_{61}. Figure 3 is a 4×4 Å^2 constant-height image. The scale bar to the right monitors the logarithm of the current. We see that there are no discernible effects of boundaries and we notice a striking resemblance with the reported experimental results of Hallmark *et al.*[2] The brighter points correspond to the atomic positions of Au atoms in the (111) plane. Each atom appears to be about 2.3 Å wide. The current is lower between two adjacent atoms (bridge sites). There is a slightly deeper current drop at the threefold hollow sites.

In Table II we report the calculated topographical corrugation for Au_{91} obtained with the experimental bias voltage (30 mV at tip) and set point current (3 nA) for

TABLE II. Effect of tip structure and of the dephasing rate α on the base-line tip height z_0 and the topographical corrugation Δz_0 in Au(111). The tip is modeled as a cluster with an apex atom. In the two upper layers, atoms occupy the lattice positions of Au and W (111) planes, respectively. In the W tip with an overlayer of Au atoms, the Au atoms substitute W atoms in the respective positions of the W. The substrate is modeled as a single layer cluster Au_{91}. The set point current is 3 nA and the tip bias voltage -30 mV, as in Ref. 2.

Tip apex	Tip (second layer)	Tip (third layer)	z_0 (Å) ($\alpha=1$ eV)	Δz_0 (Å) ($\alpha=1$ eV)	z_0 (Å) ($\alpha=0.1$ eV)	Δz_0 (Å) ($\alpha=0.1$ eV)
Au			3.93	0.12	3.85	0.22
Au	Au_3		4.67	0.13	4.80	0.09
Au	Au_3	Au_7	4.36	0.15	4.49	0.12
W			4.95	0.13	5.03	0.11
W	W_3		4.70	0.07	4.65	0.06
W	W_3	W_6	4.81	0.07	4.83	0.10
Au	W_3	W_6	4.35	0.11	4.38	0.11
Au	Au_3	W_6	4.17	0.18	4.13	0.24

Au(111). The topographical corrugation for $\alpha=1$ eV turns out to be between 0.06 and 1.8 Å. By comparison, the experimentally observed corrugation is 0.05–0.3 Å.[2] The different values in Table II correspond to different models of atomically sharp tips having *s*-wave and *d*-wave character at the tip apex. We have used these various models in order to provide a comparison with the theory of Chen,[19] where the enhanced corrugation is attributed to a *d*-wave tip. His hypotheses are consistent with the *d*-band metal tips commonly used in these experiments.[2,14] The microscopic structure at the tip apex is, however, not exactly known. One of the advantages of the cluster approach is that it allows us to infer the kind of tip used during an actual experiment.[14] Each tip in our calculations is atomically sharp and the atoms are arranged within three layers, each layer having the lattice parameters of the (111) plane of the corresponding element. For Au, 2.884 Å is the nearest-neighbor distance and the interlayer spacing is 2.335 Å. For W, 3.165 Å is the bcc cell side and 1.827 Å is the interlayer distance. The last two rows of Table II refer to an overlayer model of the tip, where Au atoms substitute W atoms in the respective lattice positions. It appears that tips with a Au atom at the apex enhance the corrugation significantly in comparison to tips made of Au or W. This result appears to be compatible with the direct observation made by Wintterlin *et al.*[24] that removal of atoms from the substrate occurs during *in situ* sharpening by field desorption and that it is only after such sharpening that atomic resolution is achieved on metal surfaces. The possibility that an overlayer of substrate atoms could enhance the corrugation has been advanced earlier,[25] the mode suggested being mechanical amplification of the tip-substrate interaction due to adhesion forces. Our calculations provide the alternate suggestion that the observed contrast could arise almost entirely from electronic energy mismatch between localized levels. Tips with a homogeneous chemical composition still produce a corrugation within the vertical resolution of a STM, but to a significantly lesser extent. Moreover, our model suggests that presence of higher angular momentum orbitals at the tip apex is not a necessary condition for getting atomic resolution on low-index metal surfaces.[19]

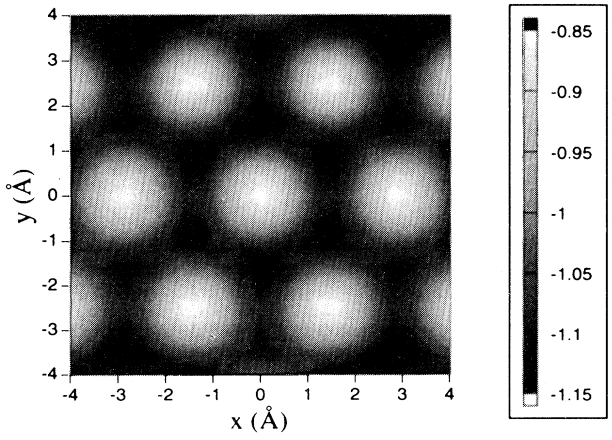

FIG. 3. Contrast in the constant-height image of Au(111), modeled as a single-layer Au_{97} cluster. The current maxima are at the atom positions. The single atom tip scans at 4 Å above the plane. The scale bar shows the value of $\log_{10}(I/nA)$.

The corrugation can also be enhanced significantly by a decrease in α. From Table III, the average base-line height z_0 turns out to be always within the range 4–5 Å and to exhibit a slight tendency to increase (by a few tenths of an angstrom) when α gets smaller. This is a consequence of a coherence enhancement in conductance. The corrugation is calculated as the difference in height between the average of two adjacent maxima and the minimum in between. Those cases in which the difference between the maxima is greater than 0.05 Å have been rejected and the corrugation recalculated. The recalculation in these cases is done by taking the height of the atoms at (2.884,0,0) and (5.768,0,0) Å and, if further necessary, by enlarging the cluster size to Au_{127}. The corrugation remains approximately the same, with only two noticeable effects, both involving a Au atom at the tip apex: the single Au atom tip, for which an increase of α by one order of magnitude doubles the corrugation (0.21 Å in comparison to 0.11 Å at $\alpha=1$ eV), and the Au overlayer on the W tip for which the corrugation increases up to 0.24 Å. These data are consistent with

TABLE III. EHT screening parameters (ξ_1) and ionization potentials (IP) for Slater-type orbitals of adatoms.

	H		C		O		Na	
Orbital	ξ_1 (a.u.)	IP (eV)	ξ_1 (a.u.)	IP (eV)	ξ_1 (a.u.)	IP (eV)	ξ_1 (a.u.)	IP (eV)
1*s*	1.3	−13.6						
2*s*			1.625	−21.4	2.275	−32.3		
2*p*			1.625	−11.4	2.275	−14.8		
3*s*							0.733	−5.1

the idea that the overlayer is responsible for the atomic resolution in low index metals and they point to the fact that coherence effects can significantly enhance the apparent corrugation. The good agreement between the predictions of these cluster models and experiment can be attributed also to the localized nature of surface states in Au(111).[2] In a forthcoming paper, we plan to discuss the possible role of overlayers in contact resistance experiments[26] in providing a possible explanation of observed *I-z* characteristics.

III. IMAGES OF ADSORBED ATOMS

In this section and the next, we present calculated images of simple adsorbates on the Au(111) substrate and attempt to address the essential features of systems studied in actual STM experiments with atoms and small molecules. We consider adsorbed atoms in this section. We begin our study with Au, Na, and H. This choice of adsorbates allows us to study energy mismatch effects. In the images shown below, the scale bar shows the value of $\log_{10}(I/nA)$.

A. Au, Na, and H on Au(111): Energy mismatch

For the present purpose, we choose adatoms that are represented by a single orbital. In addition to Au as the adsorbate, we will consider Na and H, whose on-site energies, taken as the respective experimental ionization potentials, lie, respectively, above and below the Fermi level of the Au substrate with comparable energy mismatch. The ionization potentials of Na and H are −5.1 (3*s*) and −13.6 (1*s*) eV, respectively, while the Au 6*s* ionization potential is −9.22 eV.

We take the tip as scanning 5 Å above the (111) plane. In Fig. 4(a) the image of a Au adatom adsorbed on the hollow site (0,+1.665,2.335) Å on the Au_{97} cluster is shown. We have here an example of tunneling through an adsorbate level that lies close to the Fermi level of the metal electrodes. The Au atom appears as a protrusion 8 Å wide and the current increases by three orders of magnitude above the adsorption site. When the tip is above the hollow site, the Au atom is approximately halfway between the tip and the substrate. One expects a large enhancement of the current on the basis of resonant tunneling considerations as pointed out by Lindsay *et al.*[27] For a set point current of 1 nA and 20 mV tip bias voltage, the height above a Au atom in the plane at (5.768,0,0) Å is 4.62 Å and on top of the Au adatom it is 7.07 Å, so that the 2.45-Å corrugation overestimates slightly (0.11 Å) the actual topography.

In Fig. 4(b) we show the image of a Na atom adsorbed on the hollow site (0,+1.665,2.3) Å of Au_{97}(111), where the value of the *z* coordinate for Na, taken from low-energy electron-diffraction (LEED) data of a Na mono-

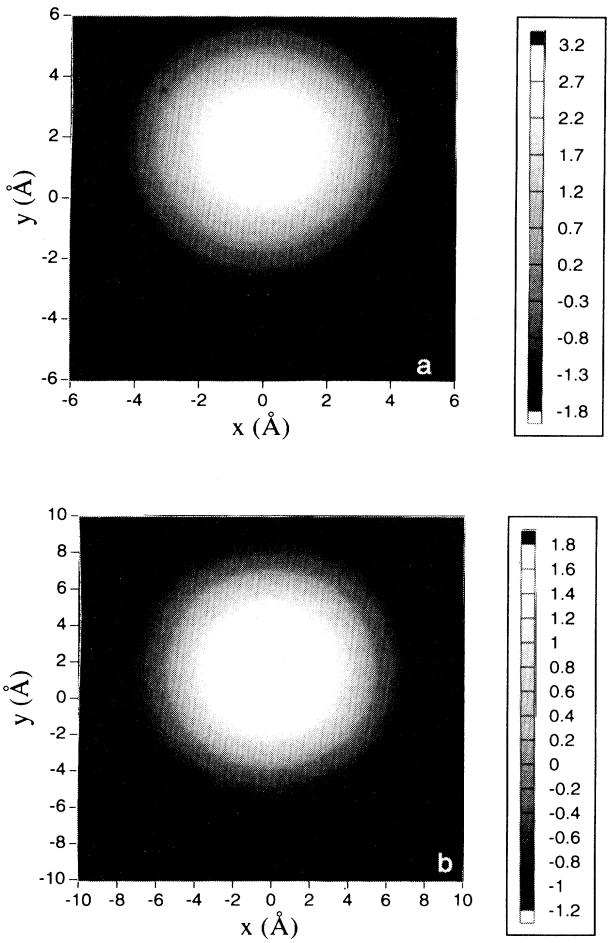

FIG. 4. Comparison between the images of tunneling current for two different adatoms, adsorbed in the hollow site of Au_{97}(111), at (0,1.7,2.3) Å: (a) Au and (b) Na. The single-atom Au tip scans 5 Å above the plane of Au atoms. The enhancement of the current at the adsorption site with respect to the surface is approximately 3 orders of magnitude for the Au adatom and 1.8 orders of magnitude for the Na adatom. Notice the different scanning area and the lateral spread of the current around the adsorption site, which reflects the different radial decay of the adatom level wave function.

layer on Al(111),[28] matches that of the Au atom. As a result of the energy mismatch, the current on top of the Na atom increases by less than two orders of magnitude with a lateral spread of ~ 16 Å. This means that the influence of the Na adatom on the current extends to about four neighbor shells of surface Au atoms. This stems from the fact that the $3s$ orbital decays rather slowly with a characteristic distance ≈ 0.73 a.u. The corresponding corrugation (3.5 Å) overestimates the actual topography because of the excessively slow decay of the Na wave function outside the surface in the EHT parametrization. These features are in qualitative agreement with *ab initio* calculations by Lang[3] in which Na appears as a protrusion 1.6 Å high and 16 Å wide at the base.

Figures 5(a) and 5(b) show images of a H atom adsorbed at the hollow site $(0,+1.665,0.6)$ Å of Au_{97} for two different substrate-tip distances. The z coordinate is taken from cluster calculations of adsorption of small atoms onto transition metals available in the literature.[4,7] For the tip scanning at 5 Å, there is an increase in the tunneling current at the location of the adsorption site [see Fig. 5(b)]. The three next neighbor atoms appear brighter than the other Au atoms.

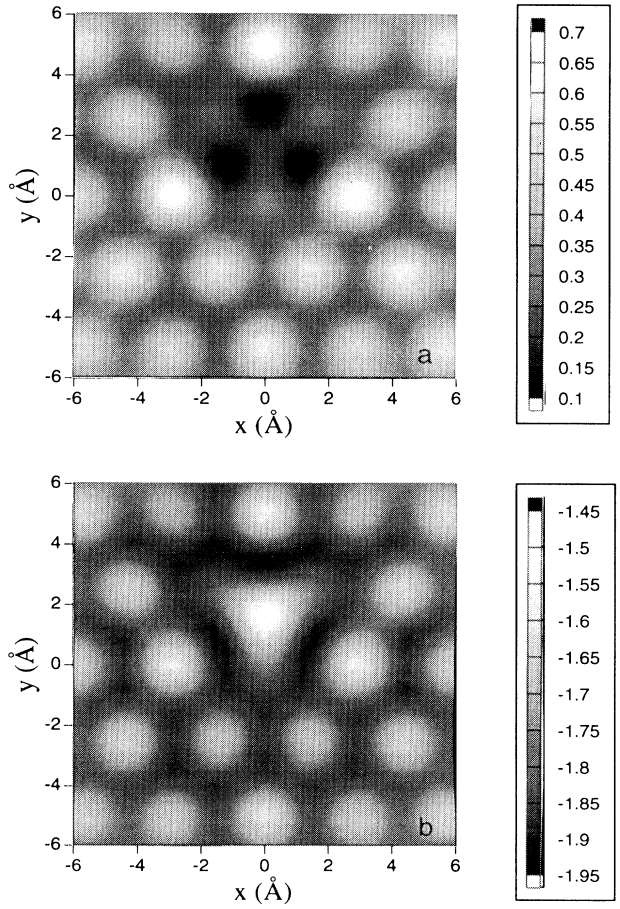

FIG. 5. Disappearance of adatom features as the tip-substrate separation decreases is exhibited for a H atom adsorbed in the hollow site of $Au_{97}(111)$ at (0,1.7,0.6). The tip scans at (a) 4 Å and (b) 5 Å above the plane of Au atoms. The enhancement of the current in correspondence of the three next neighbors indicates that the effect of the adsorption extends about 3.5 Å from the adsorption site.

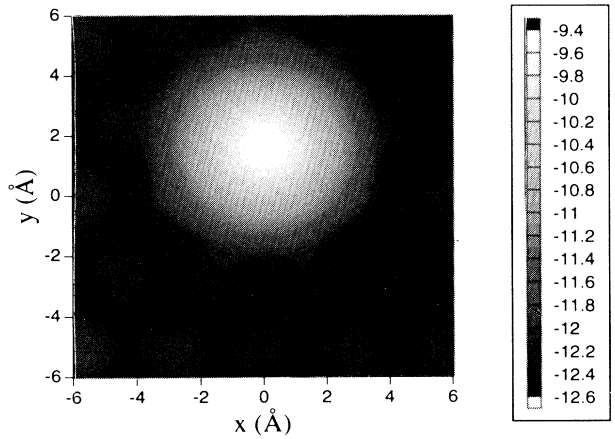

FIG. 6. Total electron density map at 5 Å for a H atom adsorbed in the hollow site of $Au_{97}(111)$ at (0,1.7,0.6).

The energy difference between the adatom resonance and the substrate Fermi level is an important factor that determines the appearance of the images.[3] Thus H appears to be smaller not only because it sits closer to the surface than Au and Na, but also because the $1s$ level in H (-13.6 eV) lies far apart in energy from the Fermi level (-8.4 eV), whereas the energies are closer to the Fermi level for Au (-9.22 eV) and Na (-5.1 eV). We have constructed maps of the local density of states at the Fermi level (which we do not present here) that are analogous to the images in Figs. 4 and 5(b) and found them to be in agreement with the predictions of the transfer Hamiltonian theory.[3,22] The demonstration of Tersoff and Hamann[22] that, in the case of bare surfaces, the local density of states at the Fermi level and the total density have similar features agrees with our calculations in the case of Au and Na adatoms, but not in the case of H (Fig. 6). This is compatible with the results of Lang.[3] The larger spread of the electron density with respect to the local density in Fig. 6 arises from two factors: (i) the H resonance at the Fermi level mixes mainly with Au nearest-neighbor orbitals, i.e., the bonding is localized, and (ii) the total electron density for H is larger than in the case of Au and Na because the $1s$ level lies mainly below the Fermi level: the H atom has gained one extra electron from the metal.

B. C and O on Au(111): Inversion and nontopographical holes

Experiments by Brune *et al.*[4,5] have uncovered the interesting phenomenon that the contrast at the adsorption site can change from a protrusion to a hole when the bias voltage is decreased. In a low-voltage regime under constant-current conditions, this implies that the average gap distance has decreased. Our calculations for H adsorbate (see Sec. III A above) show an inversion of con-

trast from bump [Fig. 5(b)] to hole [Fig. 5(a)] when the tip distance is decreased to 4 Å. Four main features are distinguishable in Fig. 5(a): (i) the H adatom is transparent, (ii) the current on top of the three nearest-neighbor Au atoms is lowered with respect to further Au atoms, (iii) the current above the three hollow sites adjacent to the adsorption site is strongly depleted, and (iv) the current on top of the three next neighbors is enhanced. These features which appear in our calculations for H, resemble those observed experimentally for C (Ref. 4) and O (Refs. 5, 6, and 8) adatoms on Al(111), Ni(100), and Cu(110). We therefore undertook an analysis of C and O adsorbates. Our findings are discussed in this subsection.

We calculated the constant-height image of a single C atom adsorbed at the hollow site of Au_{97}, 0.7 Å above the plane of Au atoms. A second layer of 19 Au atoms centered at (0,1.665,−2.335) Å was added in order to make it possible to discriminate between the occupied tetrahedral and empty octahedral hollow sites. The projected density of states for C (Fig. 7, left) shows that the *s* and *p* resonances are sp^3 hybridized. This means there is a dangling bond of the adatom protruding outwards from the surface. Since the C resonances in Fig. 7 lie below the Fermi level −8.7 eV, there is a large negative charge transferred to the adatom from the metal. Our findings regarding the dependence of the image on the tip substrate separation with the tip scanning at 5 Å [Fig. 8(b)] are as follows: (i) the adsorption site appears as a protrusion 4 Å wide with the result that the three nearest-neighbor atoms are not resolved; (ii) the three next neighbor Au atoms are slightly brighter than the Au atoms further away from the adsorption site; and (iii) the region in the proximity of the three hollow sites adjacent to the adsorption site exhibits a threefold depression ring. If we take the experimental parameters ($I=41$ nA, $V_T=-70$ mV), the apparent topographical height are 0.55 Å for the C atom, 0.05 Å for next neighbor Au atoms, and −0.14 Å for the empty hollow site. These results agree satisfactorily with the experimental values 1 Å for the C atom, 0.2 Å for next neighbors, and −0.2 Å for the hcp hollow sites measured on Al(111).[4] For the tip scanning at 3.5 Å [Fig. 8(a)] our calculation shows inversion of features: (i) a hole appears at the adsorption site, (ii) the current above the hollow sites is slightly depleted, and

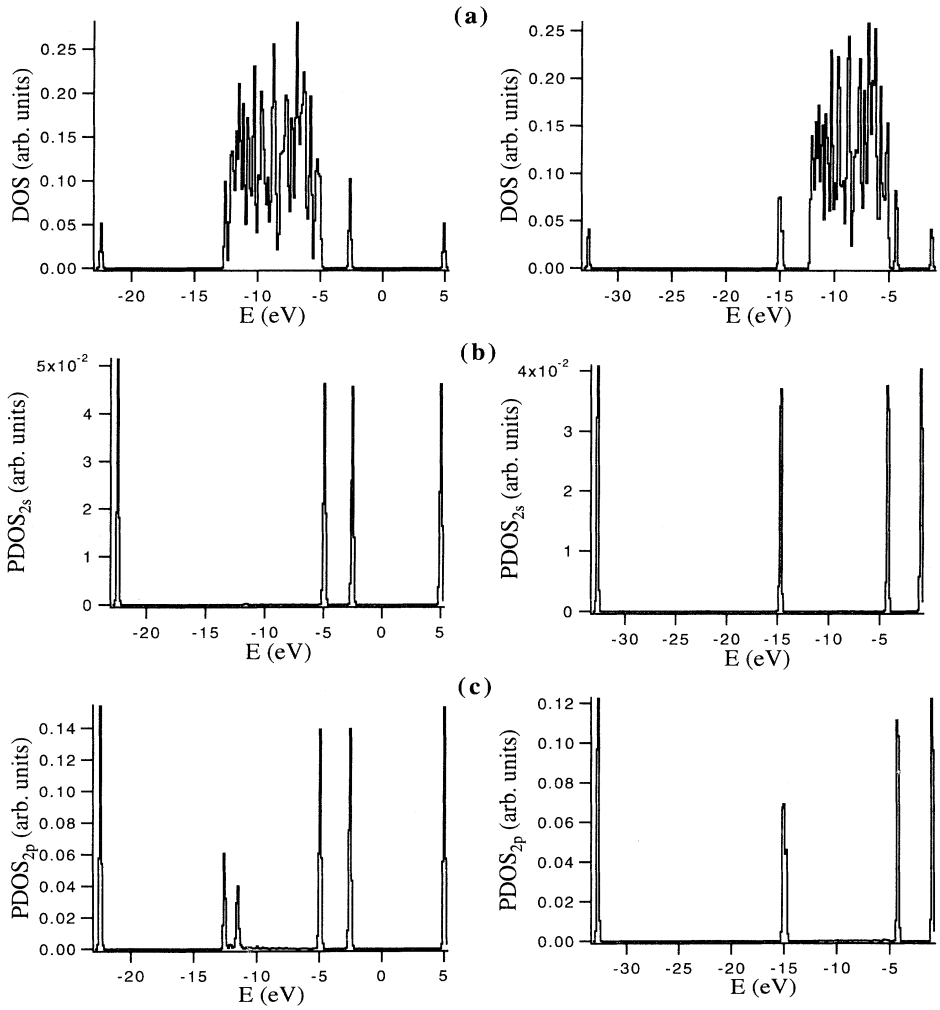

FIG. 7. Comparison between density of states of C (left column) and O (right column) adsorbed on the hollow site of Au_{97} at (0,1.7,0.7) Å: (a) density of states, (b) 2*s* projected density of states, and (c) 2*p* projected density of states.

(iii) the current above the next neighbors is enhanced. For $I=41$ nA and $V_T=-20$ mV the topographical corrugations in Fig. 8(a) are -0.7 Å at the hollow site, 0.1 Å at the nearest neighbor, -0.1 Å at the adjacent hollow site, and 0.1 Å at the next neighbor. The inversion of features occurs within 0.3-Å variation of the average tip-substrate separation 4 Å. The experimental counterpart on Al(111) exhibits nearest neighbors depressed by about -0.3 Å and next neighbors raised by 0.2 Å. The observed contrast in the case of C on Al(111) has been related by Brune *et al.*[4] to the arguments of Lang and Williams[29] that involve Friedel oscillations of the electron density in the proximity of a strongly electronegative adsorbate.

Our calculations for O as adsorbate show similar features. The main difference between the C projected density of states and the O projected density of states in Fig. 7 consists in resonances of the O adatom lying considerably below the Fermi level and the consequent transfer of two electrons from the metal to the O. As O is hybridized sp^3, a large part of the adatom charge sits on nonbonding orbitals. The O traps two metal electrons in a localized state with the consequence that the image appears as a nontopographical hole (Fig. 9). What is striking is the fact that the O adatom does not exhibit inversion of contrast when the tip substrate separation is increased. Furthermore, the constant-height image for the tip scanning 4 Å [Fig. 9(a)] reveals the presence of a small protrusion inside the adsorption site, while the protrusion disappears as the tip is retracted. Figure 9(b) shows the image corresponding to the tip scanning at 6 Å. Given the fact that the order of magnitude of the current is, in this case, below the sensitivity of the instruments, we can infer that O retains the nontopographical hole at the adsorption site throughout the relevant range of separations. These results of our calculations have considerable similarity to experimental observations[6] reported in the case of O on Ni(100).

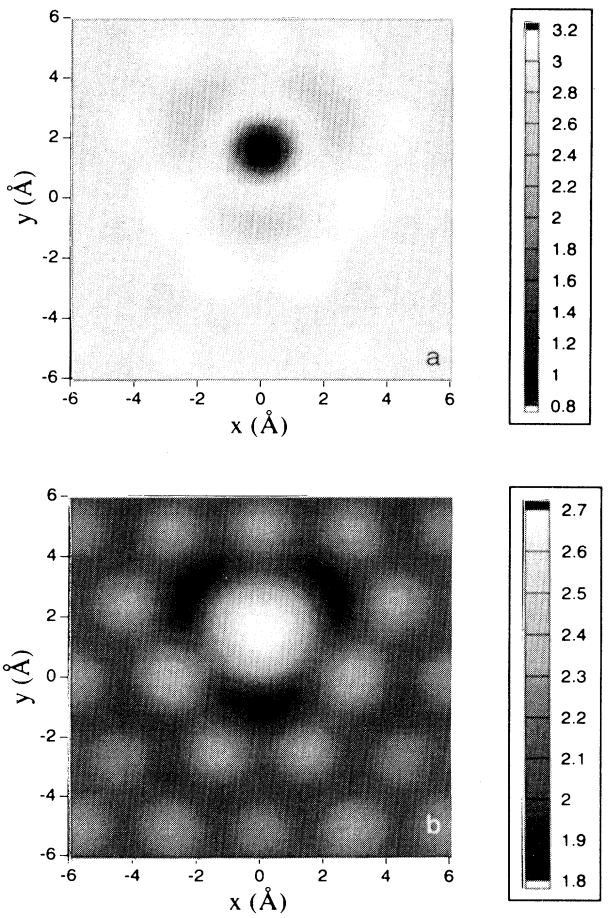

FIG. 8. Inversion of features from hole to protrusion as the tip-substrate separation increases, for a C atom adsorbed at the hollow site of $Au_{97}(111)$ at (0,1.7,0.7). The tip scans at (a) 3.5 Å and (b) 4 Å above the plane of Au atoms.

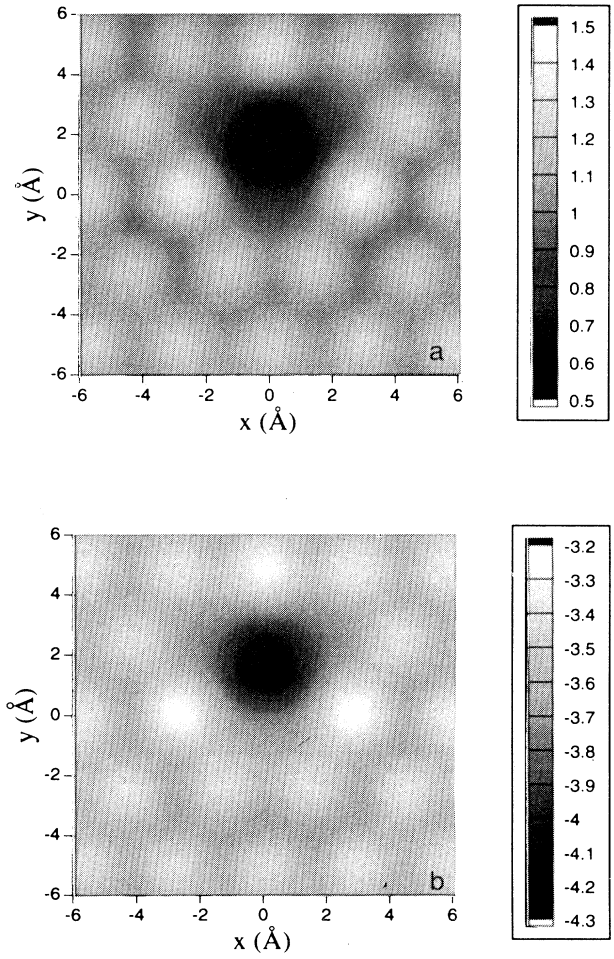

FIG. 9. Retention of nontopographical features (hole) for an O atom adsorbed at the hollow site of $Au_{97}(111)$ at (0,1.7,0.7). The tip scans at (a) 4 Å and (b) 6 Å above the plane of Au atoms. Notice the enhancement of the current at the three next neighbors, the transparency of the three nearest neighbors, and the disappearance of the smaller protrusion at the adsorption site as the tip is retracted.

Our preceding analysis suggests that nontopographical holes might be related to resonances in the adatom below the Fermi level and that nontopographical features could thus constitute a chemical "fingerprint" of adsorbates. Our suggested explanation is based on the interference features of our theory presented in detail in I. The interference occurs between direct tip-substrate and adsorbate-mediated tunneling. Other explanations have been put forward by Lang[3] on the basis of the depletion of the density of states at the Fermi level and by Doyen *et al.*[7] on the basis of the idea that a hole at the adsorption site arises when the tip is sufficiently close to probe the oscillatory part of the surface wave function.

IV. IMAGES OF ADSORBED MOLECULES

Our purpose in this section is to calculate images for simple molecular adsorates with attention on several features including the effects of the orientation of the molecule on the surface. We choose O_2 and CO as relatively simple molecules and benzene as the prototype of more complex molecules.

In Fig. 10 we show the STM images of an O_2 molecule adsorbed on the top site of Au(111). For the molecule lying flat 2 Å above the plane of Au atoms [Fig. 10(a)], the symmetry of the image clearly suggests the presence of a twofold species ("dumbbell"). The O atoms sit at ($\pm$0.7,0,2) Å in proximity of the maximum intensity, but the single atoms are not resolved. The apparent length of the molecule along the symmetry axis is approximately 5 Å. This overestimates considerably the actual bond length of 1.4 Å. The molecule adsorbed perpendicular to the surface [Fig. 10(b)] appears to be circular with a 4 Å diameter (see Fig. 9) and a slight depression is produced at the center of the adsorption site ("doughnut" shape). Arguments similar to those presented in the preceding section suggest that the hole represents an interference effect contributed by the σ bonds in the molecule lying much below the Fermi level.

Experiments[9,30] on single molecules of CO adsorbed on Pt(111) show that there is a difference according to whether CO sits on the top site or the bridge site, respectively.[30] In particular, at 1 nA current and -0.1 V tip bias voltage, the top site exhibits a 0.4-Å-high bump with a relatively flat top ("mesa") and a 7-Å lateral spread. In the bridge site, the molecule appears to be 0.14 Å high and with a sharper top ("sombrero"). The molecule appears about 6 Å wide and shows a moat around the base. We have tried to reproduce these features from our theory. The results are presented in Fig. 11. In our model, the C-O distance is taken as 1.21 Å, the C atom being closer to the metal surface. Our metal surface is a Au_{97} single-layer cluster. The carbon atom in CO is 2 Å distant from the nearest Au atom and the molecule is perpendicular to the surface. This geometry implies that the C coordinates are (0,0,2) Å for the adsorption at the top site, (0,1.665,1.3) Å for the hollow site, and (1.442,0,1.4) Å for the adsorption at the bridge site. The tip scans at $z=6$ Å on a 6×6 Å^2 area around the central Au substrate atom. Figure 11 shows the constant-height maps of the three models for CO adsorption. At the top site [Fig. 11(a)], CO appears as a protrusion about 8 Å wide and the current on top of the molecule is about three orders of magnitude larger than at the base. This corresponds to a topographical corrugation equal to 2 Å. At the center the current is slightly depleted and flattened around, resembling the observed mesa structure.[30] The mesa top has a diameter of about 3 Å. In the adsorption at the bridge site [Fig. 11(b)], CO appears to be larger (10 Å), with an increase in current of one order of magnitude, corresponding to a corrugation significantly lower (1.8 Å) than on the top site. The top of the bump is sharply peaked as in the sombrero structure.[30] Some resemblance to the moat structure[30] is present also: a circular zone is seen between the first and the second shell of neighbors around the adsorption site.

The last adsorbate in our calculations is a single benzene molecule on Au(111) at the hollow site. Experimental findings reported in the literature are as follows. Ben-

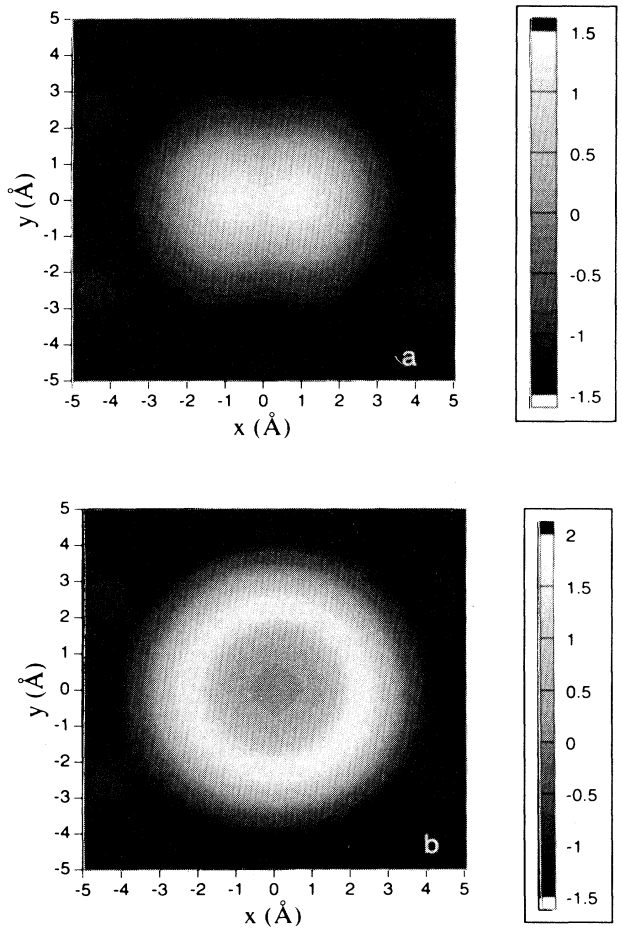

FIG. 10. Different orientations of O_2 molecule adsorbed at the top site of Au(111) are resolved: (a) flat dimer, with O atoms at ($\pm$0.7,0,2) Å, and (b) perpendicular dimer, with O atoms at (0,0,2) and (0,0,3.4) Å. The tip scans 5 Å above the Au_{43} surface. The depression at the center of the adsorption site in Fig. 8(b) arises from interference effects due to the close proximity of the Au tip atom to the upper O atom.

zene monolayers coadsorbed with two CO molecules on Rh(111) have been characterized by LEED (Ref. 31) and STM.[10] The STM images show benzene molecules as objects about 2 Å high, with no resolution of internal structure for high bias voltages. For lower bias voltages, the molecules appear as threefold structures with a depression at the center. Our theoretical images have been calculated for a single benzene molecule on the hollow site 2.2 Å above the metal surface,[31] modeled as a double-layer $Au_{97}+Au_{19}$ cluster. The molecule has D_{6h} symmetry, with a C-C distance equal to 1.42 Å. The images are acquired with the tip scanning at 5 Å [Fig. 12(a)] and 6 Å [Fig. 12(b)]. In the calculations shown in Fig. 12(a), the molecule appears to be hexagonal and 9 Å wide. At the center of the hexagon, the current drops smoothly to produce a hole at the position of the hollow site. At 6 Å, the molecule appears to be almost 12 Å wide and the shape is hexagonal. The most prominent feature is the appearance of the three bright lobes around the center of the benzene molecule. The current at the center appears depressed. The lobes stretch between the nearest-neighbor Au atoms and the nodal planes coincide with the σ_d symmetry planes of benzene. The location of the maxima, their symmetry, and the presence of the central hole are in qualitative agreement with experiment[10] and with the scattering calculation by Sautet and Joachim.[13] The hexagonal shape in the outer part of the image is at variance with the experimental evidence,[10] but we believe this can be due to either the small size of the substrate second layer or the choice of the Fermi level.[13]

V. CONCLUDING REMARKS

The primary content of this paper is calculated STM images for atomic and molecular adsorbates on the basis of our theory presented in I, in particular Eq. (1.1) for the STM current. The extended Hückel theory and the stochastic Liouville equation within the context of a cluster

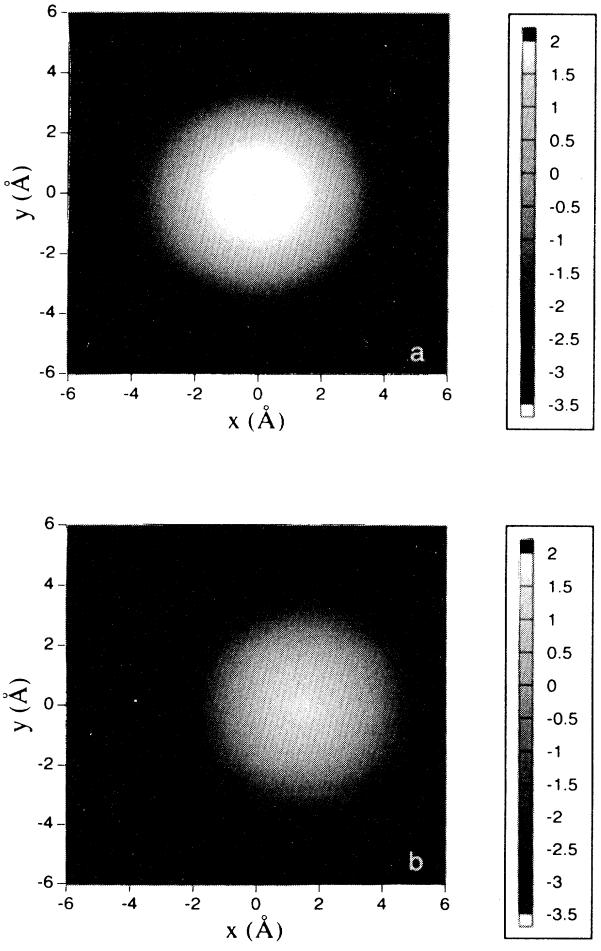

FIG. 11. Sensitivity of the current to the adsorption site for a CO molecule adsorbed (a) at the top site and (b) at the bridge site. The tip scans 5 Å above the (111) plane of Au_{97}, CO stands always upright, with C closer to the Au surface, at a distance of 2 Å from the nearest Au atom. CO bond length is 1.21 Å.

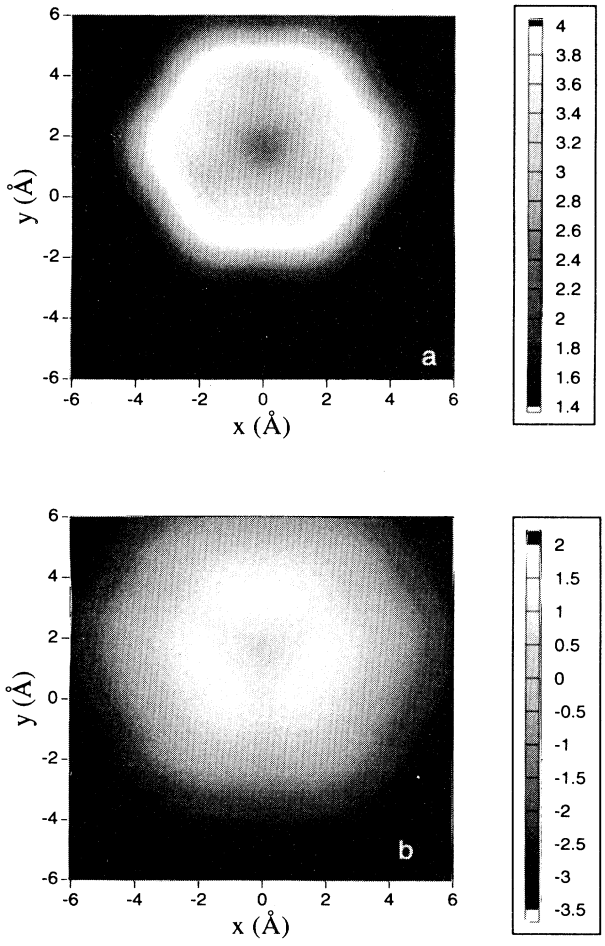

FIG. 12. Change of contrast with tip-substrate separation for benzene adsorbed at the hollow site of Au (111): (a) 4 Å and (b) 6 Å. The benzene ring is parallel to the surface (2.2 Å above) and C and H atoms are taken to be coplanar. The substrate is modeled as a two-layer slab, the surface layer is Au_{97}, and the layer beneath is Au_{19} whose center atom is underneath the hcp threefold hollow site. The tip bias voltage is −0.1 V.

model have provided the calculational tools for the propagators to be fed into (1.1). The treatment of arbitrary degree of coherence allowing us to address the entire range between perturbative and nonperturbative limits has been a special feature of our calculations. In addition to the agreement with experimentally reported STM images of known substrates, we have found the following features in our study of adsorbates.

In the case of absorbed atoms, we have (i) shown that the appearance of holes in the images can be explained in terms of interference effects related to energy mismatch between the adatom and the substrate Fermi level; (ii) obtained inversion features for C and retention of the nontopographical hole for O, both in qualitative agreement with experiment; and (iii) shown that, for large tip distances, the LDOS map resembles the STM image, but the total electron density map does not when the adatom level is below the Fermi level, in agreement with *ab initio* arguments. In the case of adsorbed molecules, we have found that (i) the adsorbed molecules appear to be considerably larger than their actual size and have a different appearance for different adsorption sites; (ii) while some submolecular resolution is possible in molecules adsorbed flat, it is difficult to locate the atoms directly from the image; and (iii) in the case of benzene, our images show a three-lobed pattern with the lobes extending between the underlying substrate atoms as seen experimentally and conjectured earlier theoretically.

One of the ingredients of our calculational scheme is the stochastic Liouville equation with its simple treatment of coherence in electron transport through the single dephasing rate. The generalization of the analysis is planned to be reported in the near future. The other ingredient in our calculations is the extended Hückel theory. In the context of STM images, EHT has already been applied to the calculation of transmission probability through a tip-adsorbate-substrate junction[13] and a metal-adsorbate local density of states.[32] The advantages of EHT are that it is a simple noniterative framework for calculating the electronic structure of large and complicated systems and that it has already led to a number of established results for configuration, surface bonding, energetics of the adsorption site, and cluster size effects in chemisorption.[12] The shortcomings of the EHT consist of some arbitrariness in the choice of parameters and the unsatisfactory description of the one-electron Hamiltonian at large separations. We plan to replace the EHT by *ab initio* calculations in the manner of Fischer and Blöchl[33] in the near future. We hope that, in these extended versions, our theory will be able to address realistic issues such as tip-sample and tip-substrate interaction effects.[34,35]

ACKNOWLEDGMENTS

We would like to thank A. Gibson for discussions and A. Degli Esposti for assistance in optimizing the simulation code. The calculations were performed on an IBM RISC 6000 530 H of ISM, CNR. One of us (F.B.) acknowledges Consorzio Technobiochip–Istituto di Biofisica CNR Pisa and Consorzio INFM–Istituto di Spettroscopia Molecolare CNR Bologna, Italy for partial support.

*Present address: Istituto di Spettroscopia Molecolare ed Istituto LAMEL Consiglio Nazionale delle Ricerche, Via Gobetti 101, 40129 Bologna, Italy.

[1]V. M. Kenkre, F. Biscarini, and C. Bustamante, Phys. Rev. B **51**, 11 074 (1995).
[2]V. M. Hallmark, S. Chiang, I. F. Rabolt, J. D. Swalen, and R. J. Wilson, Phys. Rev. Lett. **59**, 2879 (1987).
[3]N. D. Lang, Phys. Rev. Lett. **56**, 1164 (1986).
[4]H. Brune, J. Wintterlin, G. Ertl, and R. J. Behm, Europhys. Lett. **13**, 123 (1990).
[5]H. Brune, J. Wintterlin, R. J. Behm, and G. Ertl, Phys. Rev. Lett. **68**, 624 (1992).
[6]E. Kopatzki and R. J. Behm, Surf. Sci. **245**, 255 (1991).
[7]G. Doyen, D. Drakova, E. Kopatzki, and R. J. Behm, J. Vac. Sci. Technol. A **6**, 327 (1988).
[8]L. Ruan, F. Besenbacher, I. Stensgaard, and E. Laegsgaard, Phys. Rev. Lett. **70**, 4079 (1993).
[9]P. Zeppenfeld, C. P. Lutz, and D. M. Eigler, Ultramicroscopy **42-44**, 128 (1992).
[10]H. Ohtani, R. J. Wilson, S. Chiang, and C. M. Mate, Phys. Rev. Lett. **60**, 2398 (1988).
[11]A. Szabo and P. Ostlund, *Modern Quantum Chemistry* (McGraw-Hill, New York, 1989).
[12]R. Hoffmann, J. Chem. Phys. **39**, 1397 (1963); for a review on applications of EHT to surface problems, see, for instance, M. Simonetta and A. Gavezzotti, Adv. Quantum Chem. **12**, 103 (1980).
[13]P. Sautet and C. Joachim, Chem. Phys. Lett. **185**, 23 (1991).
[14]N. Isshiki, K. Kobayashi, and M. Tsukada, Surf. Sci. **238**, L439 (1991).
[15]H. Haken and G. Strobl, Z. Phys. **262**, 135 (1973); P. Reineker, in *Exciton Dynamics in Molecular Crystals and Aggregates,* edited by G. Hohler, Springer Tracts in Modern Physics Vol. 94 (Springer-Verlag, Berlin, 1982).
[16]G. Wannier, *Elements of Solid State Physics* (Cambridge University Press, Cambridge, England, 1959).
[17]V. M. Kenkre, in *Mathematical Methods for the Description of Energy Transfer,* edited by B. Di Bartolo (Plenum, New York, 1984), p. 1.
[18]The Mulliken analysis possesses the drawback that, when the approximation is applied to larger models of the STM junction, it can lead to negativity of propagators. However, this is likely to occur in a range of separations where overlaps are large, e.g., at tip-substrate separations much closer than a bonding distance. In this range, EHT may be said to break down. We prefer to employ the EHT within its validity range rather than to use other approximate projection schemes that always preserve the positive definiteness of the propagator matrix but require *ad hoc* renormalization.
[19]C. J. Chen, Phys. Rev. Lett. **65**, 448 (1990).

[20]M.-H. Whang-Bo *et al.*, *EHMACC An Extended Hückel Program* (University of Indiana Press, Bloomington, 1980).
[21]E. Clementi and C. Roetti, At. Data Nucl. Data **14**, 177 (1974).
[22]J. Tersoff and D. R. Hamann, Phys. Rev. Lett. **50**, 1998 (1983).
[23]N. W. Ashcroft and N. D. Mermin, *Solid State Physics* (Rinehart, Holt and Winston, New York, 1976).
[24]J. Wintterlin, J. Wiechers, H. Brune, T. Gritsch, H. Höfer, and R. J. Behm, Phys. Rev. Lett. **62**, 59 (1989).
[25]N. J. Zheng and I. S. T. Tsong, Phys. Rev. B **41**, 2671 (1990).
[26]J. K. Gimgewski and R. Möller, Phys. Rev. B **36**, 1284 (1987).
[27]S. M. Lindsay, O. F. Sankey, Y. Li, C. Herbst, and A. Rupprecht, J. Am. Chem. Soc. **94**, 4655 (1990).
[28]M. A. VanHove, in *The Nature of the Surface Chemical Bond*, edited by T. N. Rhodin and G. Ertl (North-Holland, Amsterdam, 1979), p. 277.
[29]N. D. Lang and A. R. Williams, Phys. Rev. B **3**, 1215 (1978).
[30]J. A. Stroscio and D. M. Eigler, Science **254**, 1319 (1991).
[31]R. F. Lin, G. S. Blackman, M. A. VanHove, and G. A. Somorjai, Acta Crystallogr. Sec. B **43**, 368 (1987).
[32]V. M. Hallmark, S. Chiang, K. Meinhardt, and K. Hafner, Phys. Rev. Lett. **70**, 3740 (1993).
[33]A. J. Fisher and P. E. Blöchl, Phys. Rev. Lett. **70**, 3263 (1993).
[34]U. Landman, W. D. Luedtke, and A. Nitzan, Surf. Sci. **210**, L177 (1989).
[35]I. P. Batra and S. Ciraci, J. Vac. Sci. Technol. A **6**, 313 (1988).

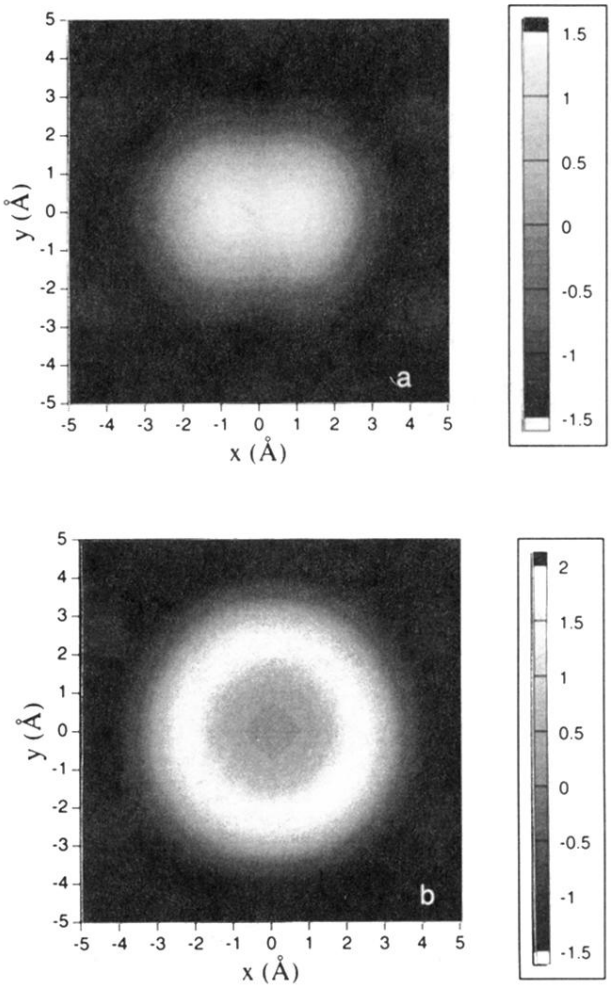

FIG. 10. Different orientations of O_2 molecule adsorbed at the top site of Au(111) are resolved: (a) flat dimer, with O atoms at ($\pm$0.7,0,2) Å, and (b) perpendicular dimer, with O atoms at (0,0,2) and (0,0,3.4) Å. The tip scans 5 Å above the Au_{43} surface. The depression at the center of the adsorption site in Fig. 8(b) arises from interference effects due to the close proximity of the Au tip atom to the upper O atom.

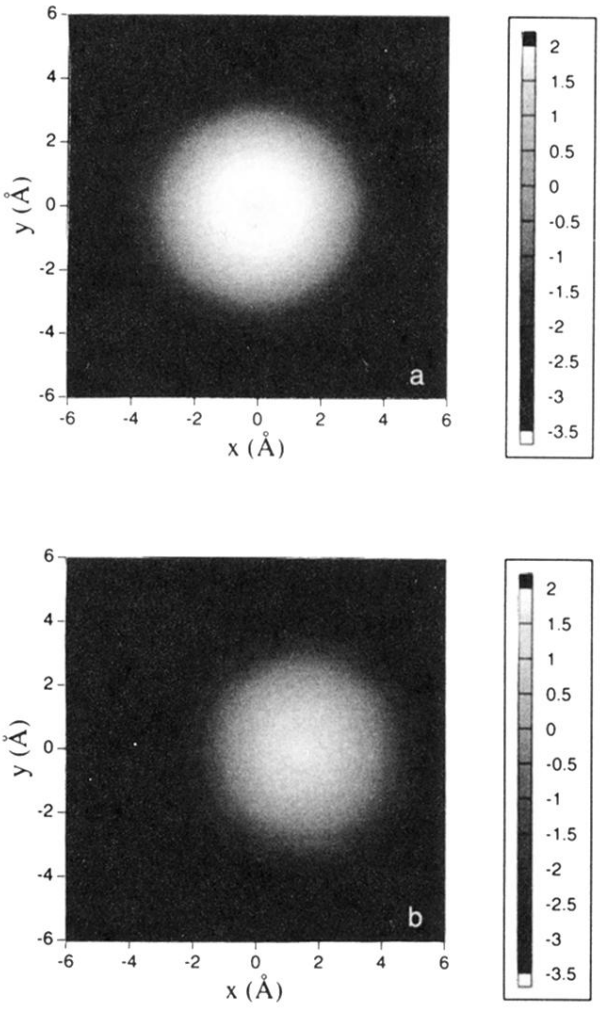

FIG. 11. Sensitivity of the current to the adsorption site for a CO molecule adsorbed (a) at the top site and (b) at the bridge site. The tip scans 5 Å above the (111) plane of Au_{97}, CO stands always upright, with C closer to the Au surface, at a distance of 2 Å from the nearest Au atom. CO bond length is 1.21 Å.

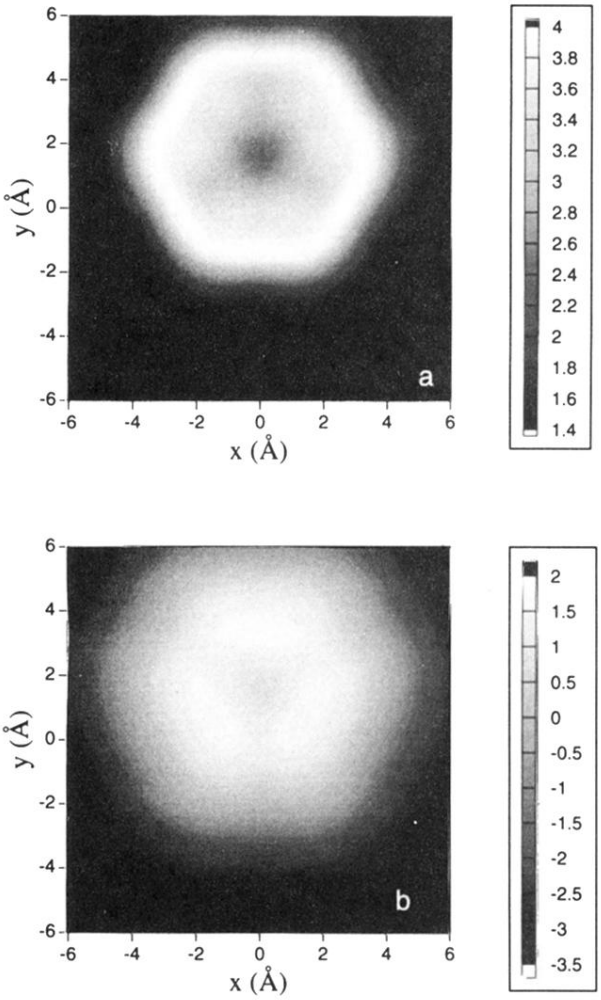

FIG. 12. Change of contrast with tip-substrate separation for benzene adsorbed at the hollow site of Au (111): (a) 4 Å and (b) 6 Å. The benzene ring is parallel to the surface (2.2 Å above) and C and H atoms are taken to be coplanar. The substrate is modeled as a two-layer slab, the surface layer is Au_{97}, and the layer beneath is Au_{19} whose center atom is underneath the hcp threefold hollow site. The tip bias voltage is -0.1 V.

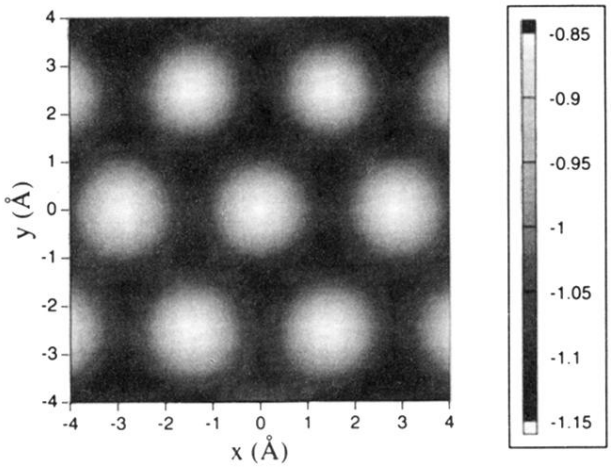

FIG. 3. Contrast in the constant-height image of Au(111), modeled as a single-layer Au_{97} cluster. The current maxima are at the atom positions. The single atom tip scans at 4 Å above the plane. The scale bar shows the value of $\log_{10}(I/nA)$.

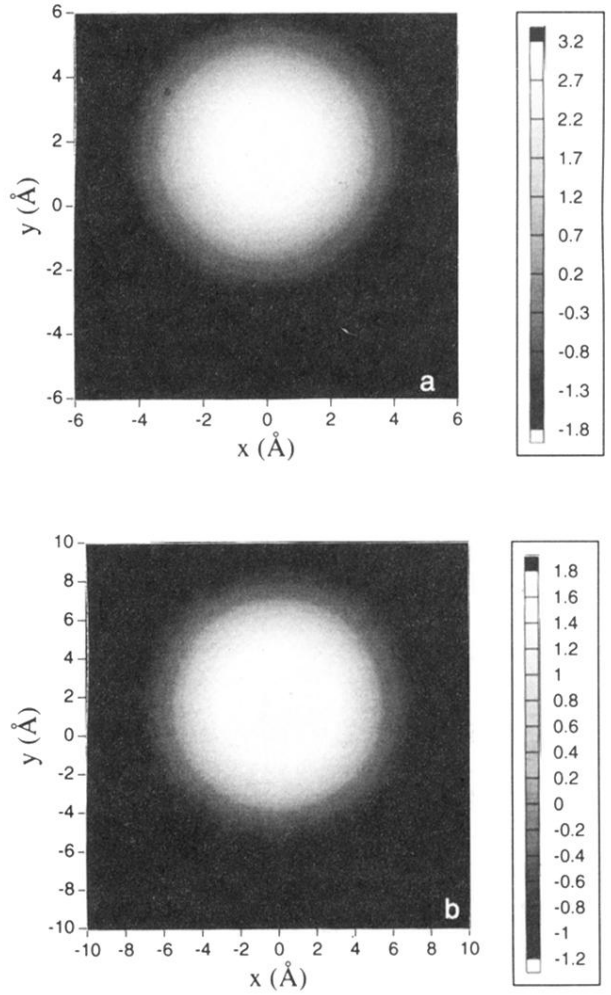

FIG. 4. Comparison between the images of tunneling current for two different adatoms, adsorbed in the hollow site of $Au_{97}(111)$, at (0,1.7,2.3) Å: (a) Au and (b) Na. The single-atom Au tip scans 5 Å above the plane of Au atoms. The enhancement of the current at the adsorption site with respect to the surface is approximately 3 orders of magnitude for the Au adatom and 1.8 orders of magnitude for the Na adatom. Notice the different scanning area and the lateral spread of the current around the adsorption site, which reflects the different radial decay of the adatom level wave function.

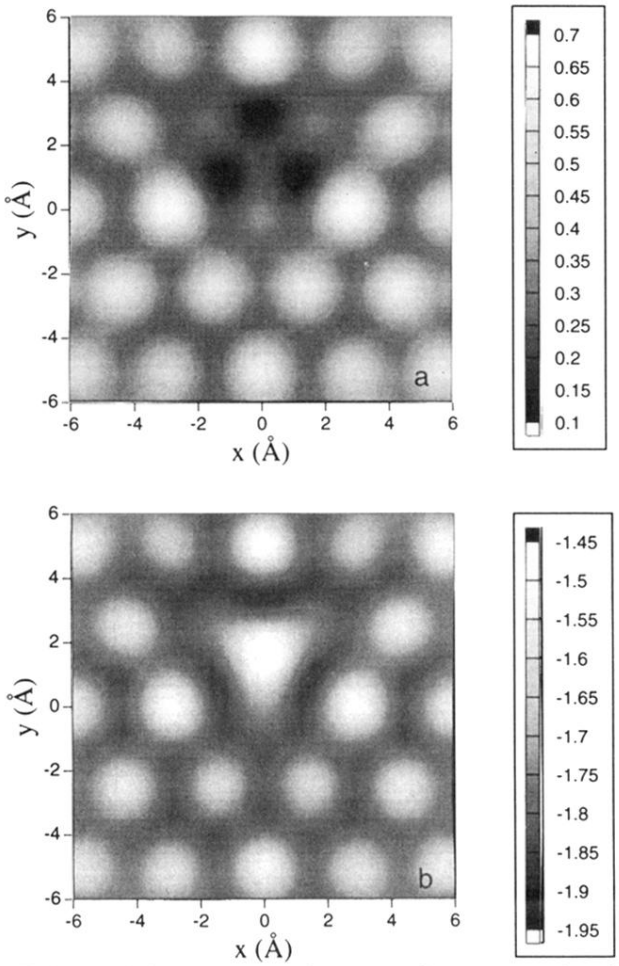

FIG. 5. Disappearance of adatom features as the tip-substrate separation decreases is exhibited for a H atom adsorbed in the hollow site of $Au_{97}(111)$ at (0,1.7,0.6). The tip scans at (a) 4 Å and (b) 5 Å above the plane of Au atoms. The enhancement of the current in correspondence of the three next neighbors indicates that the effect of the adsorption extends about 3.5 Å from the adsorption site.

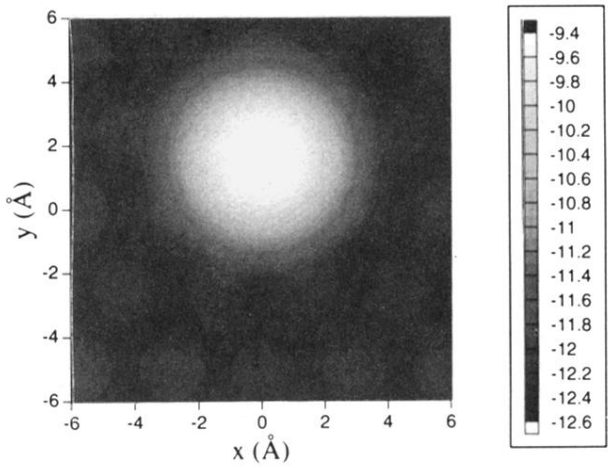

FIG. 6. Total electron density map at 5 Å for a H atom adsorbed in the hollow site of $Au_{97}(111)$ at (0,1.7,0.6).

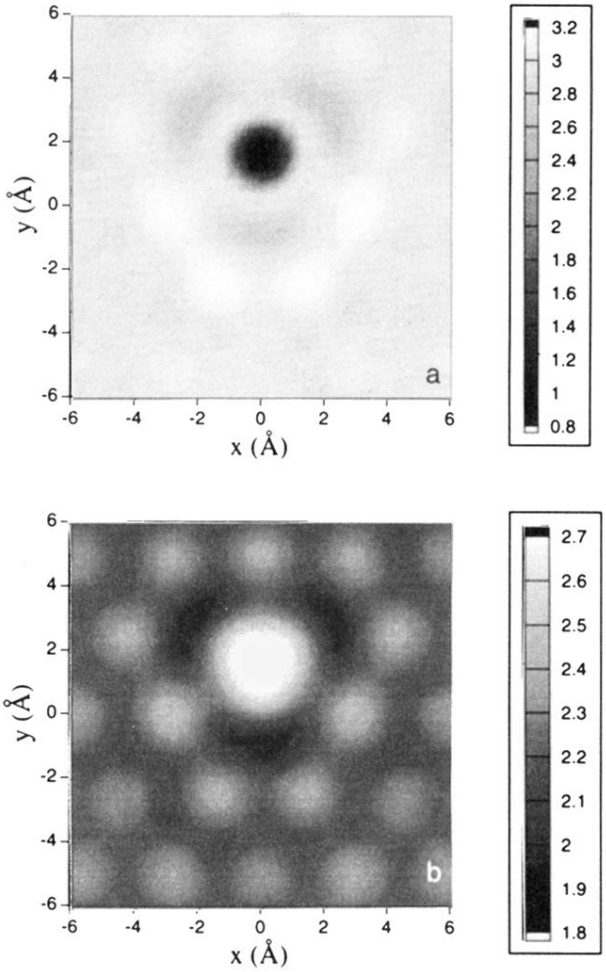

FIG. 8. Inversion of features from hole to protrusion as the tip-substrate separation increases, for a C atom adsorbed at the hollow site of $Au_{97}(111)$ at (0,1.7,0.7). The tip scans at (a) 3.5 Å and (b) 4 Å above the plane of Au atoms.

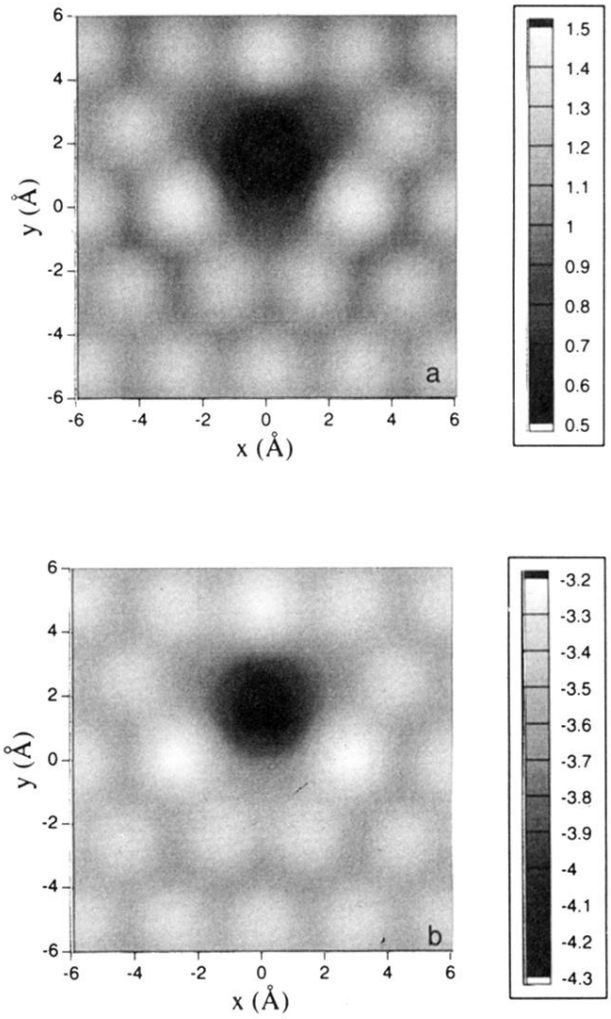

FIG. 9. Retention of nontopographical features (hole) for an O atom adsorbed at the hollow site of $Au_{97}(111)$ at (0,1.7,0.7). The tip scans at (a) 4 Å and (b) 6 Å above the plane of Au atoms. Notice the enhancement of the current at the three next neighbors, the transparency of the three nearest neighbors, and the disappearance of the smaller protrusion at the adsorption site as the tip is retracted.